Journal of Alloys and Compounds 480 (2009) 568–574

Contents lists available at ScienceDirect

Journal of Alloys and Compounds

journal homepage: www.elsevier.com/locate/jallcom

Monoclinic phases and stress-relief conditions in $(1-x)Pb(Mg_{1/3}Nb_{2/3})TiO_3$–$xPbTiO_3$ solid solutions

V.Yu. Topolov*

Department of Physics, Southern Federal University, 5 Zorge Street, 344090 Rostov-on-Don, Russia

ARTICLE INFO

Article history:
Received 11 July 2008
Received in revised form 23 January 2009
Accepted 30 January 2009
Available online 7 February 2009

PACS:
61.50.Ks
77.80.Bh
64.70.Kb

Keywords:
Ferroelectrics
Crystal structure and symmetry
Elasticity

ABSTRACT

A comparative study on heterophase states in perovskite-type solid solutions of $(1-x)Pb(Mg_{1/3}Nb_{2/3})TiO_3$–$xPbTiO_3$ is carried out for compositions near the morphotropic phase boundary. The conditions for mechanical stress relief at elastic matching of phases are analysed at x = const in a wide temperature range. The heterophase states concerned with the presence of the intermediate monoclinic phase are interpreted using the domain state–interface diagrams calculated for x = 0.28, 0.32 and 0.34. It is shown that optimum volume fraction parameters of the domains in the monoclinic phase of the B type are varied in relatively wide ranges and promote complete stress relief with cubic–monoclinic phase coexistence. Two scenarios of stress relief at x = 0.32 are considered in connection with different heterophase states (either tetragonal–monoclinic of the B type or tetragonal–monoclinic of the C type) in a wide temperature range. Possibilities of elastic matching of two polydomain phases (tetragonal–monoclinic of the B type) with almost equal relative widths of the domains in these phases are shown for x = 0.34. The active role of domains of the monoclinic phases in stress relief and forming the planar unstrained interfaces is discussed.

1. Introduction

In the last decade, perovskite-type relaxor-ferroelectric solid solutions of $(1-x)Pb(Mg_{1/3}Nb_{2/3})TiO_3$–$xPbTiO_3$ (PMN–xPT) have been intensively studied due to their remarkable electromechanical properties, intermediate monoclinic phases and various heterophase states near the morphotropic phase boundary [1]. Experimental data show that the following phases can coexist at $0.26 \le x \le 0.39$: cubic (C, Pm3m symmetry) and tetragonal (T, P4mm symmetry) [2–4], C and rhombohedral (R3m symmetry) [2,5], T and rhombohedral [2,5–7], monoclinic M_B (Cm symmetry) and monoclinic M_C (Pm symmetry) [8,9], M_C and T [3,8], monoclinic M_A (Cm symmetry) and T [10], M_A and M_C [3], T and orthorhombic [4], orthorhombic and M_B [4], and M_B and T [9] phases. Some cases of the phase coexistence on zero-field cooling were considered in recent experimental work. For example, the T and M_C phases coexist in wide temperature ranges at x = 0.32, 0.36 [11] and 0.33 [12] while the T and M_B phases coexist at x = 0.32 and 0.34 [9]. The T–M_B phase coexistence observed in unpoled PMN–xPT ceramic samples in a very wide temperature range ($\sim 10^2$ K) is the result of a local stress field and the clampdown and blocking effect [9]. These circumstances and the martensitic-like phase transitions [9] in PMN–xPT stimulate the need for an analysis of heterophase states which would appear at different scenarios of zero-field cooling or under different conditions for internal stress relief. This analysis becomes important in connection with the presence of two monoclinic phases (Pm and Cm) of the ferroelectric nature in PMN–xPT single crystals ($0.30 \le x \le 0.47$) [13] and ceramics ($0.27 \le x \le 0.34$) [11] at room temperature. As is known from work [14,15], the remarkable physical properties of the monoclinic phases in PMN–xPT are attributed to adaptive phases formed by nano-sized domains of the T phases and treated by analogy with an adaptive martensite. The aim of the present paper is to study heterophase structures in PMN–xPT, containing one of the monoclinic phases (M_B or M_C), and an evolution of these structures in wide temperature ranges. To consider the heterophase structures, we use experimental temperature dependences of the perovskite unit-cell parameters of PMN–xPT ceramics [9] and powders [11] with compositions chosen close to the morphotropic phase boundary. We apply the matrix method [4,6,10], which makes it possible to examine elastic matching of the coexisting phases with various domain (twin) structures, to determine crystallographic characteristics of interfaces separating these phases and conditions for internal stress relief in different heterophase states.

2. Domain (twin) structures and characteristics of interfaces between phases

It is assumed that non-180° domains of types I–IV are located in a head-to-tail manner (Figs. 1 and 2) and form regular lam-

* Tel.: +7 863 2975127; fax: +7 863 2975120.
E-mail addresses: v_topolov@yahoo.com, topolov@phys.rsu.ru.

0925-8388/$ – see front matter © 2009 Elsevier B.V. All rights reserved.
doi:10.1016/j.jallcom.2009.01.122

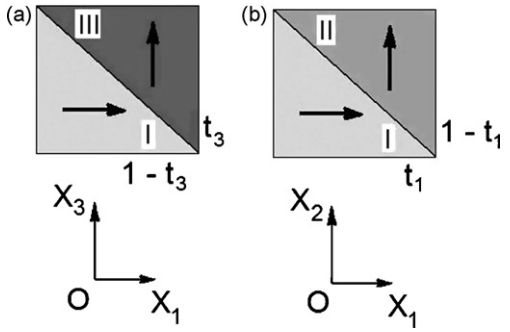

Fig. 1. Schematic drawings of ferroelectric domains (mechanical twins) of the T phase. The arrows show orientations of the spontaneous polarisation vectors $\boldsymbol{P_T^{(n)}}$ where $n = 1$, 2 or 3. The axes of the Cartesian coordinate system ($X_1X_2X_3$) are oriented parallel to the elementary translation vectors of a perovskite cell of the cubic paraelectric phase. For the domain arrangement (a), volume fractions t_3 and $1 - t_3$ are introduced, for the domain arrangement (b), volume fractions t_1 and $1 - t_1$ are introduced.

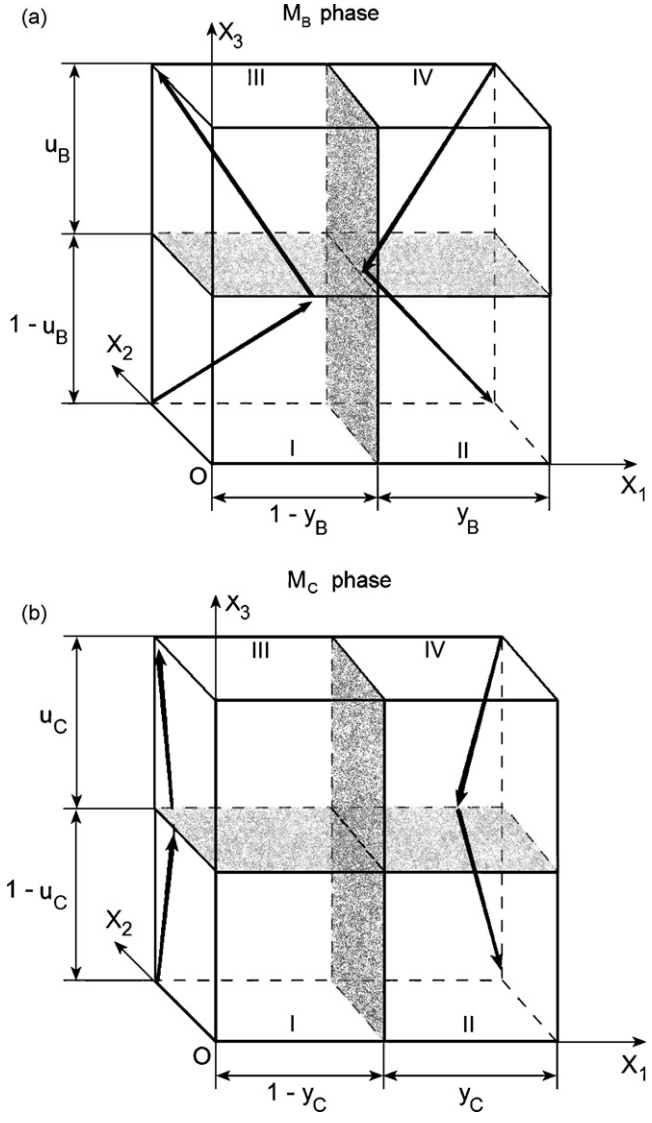

Fig. 2. Schematic drawing of ferroelectric domains (mechanical twins) of the M_B (a) and M_C (b) phases. The arrows show orientations of the spontaneous polarisation vectors $\boldsymbol{P_B^{(n)}}$ or $\boldsymbol{P_C^{(n)}}$ in the M_B (a) or M_C (b) phase, respectively ($n = 1$, 2, 3, or 4), domain walls are shaded. The axes of the Cartesian coordinate system ($X_1X_2X_3$) are oriented parallel to the elementary translation vectors of a perovskite cell of the cubic paraelectric phase. u_B, y_B, u_C, and y_C are parameters used to determine the volume fractions of the domains (see Table 1).

Table 1
Orientations and volume fractions of non-180° domains in ferroelectric phases of PMN–*x*PT.

Phases, figures	Spontaneous polarisation vectors of domains[a]	Volume fractions of domains
T, Fig. 1(a)	$\boldsymbol{P_T^{(1)}}\|\|[1\,0\,0]$ $\boldsymbol{P_T^{(3)}}\|\|[0\,0\,1]$	$1-t_3$ t_3
T, Fig. 1(b)	$\boldsymbol{P_T^{(1)}}\|\|[1\,0\,0]$ $\boldsymbol{P_T^{(2)}}\|\|[0\,1\,0]$	t_1 $1-t_1$
M_B, Fig. 2(a)	$\boldsymbol{P_B^{(1)}}\|\|[d\,\bar{1}\,1]$ $\boldsymbol{P_B^{(2)}}\|\|[1\,d\,\bar{1}]$ $\boldsymbol{P_B^{(3)}}\|\|[\bar{d}\,1\,1]$ $\boldsymbol{P_B^{(4)}}\|\|[\bar{1}\,\bar{d}\,1]$	$(1-u_B)(1-y_B)$ $(1-u_B)y_B$ $u_B(1-y_B)$ u_By_B
M_C, Fig. 2(b)	$\boldsymbol{P_C^{(1)}}\|\|[0\,\bar{g}\,1]$ $\boldsymbol{P_C^{(2)}}\|\|[g\,0\,\bar{1}]$ $\boldsymbol{P_C^{(3)}}\|\|[0\,g\,1]$ $\boldsymbol{P_C^{(4)}}\|\|[\bar{g}\,0\,\bar{1}]$	$(1-u_C)(1-y_C)$ $(1-u_C)y_C$ $u_C(1-y_C)$ u_Cy_C

[a] All the orientations are related to the perovskite unit-cell axes. It is assumed that inequalities $0 < d < 1$ and $0 < g < 1$ hold for the domains in the M_B phase and M_C phase, respectively.

inar structures in each ferroelectric phase (T, M_B and M_C). The domains being mechanical twin components are separated, according to Fousek and Janovec [16], by planar unstrained domain walls oriented parallel to the {1 1 0} planes in the T phase (Fig. 1) and to the {1 0 0} planes in the M_B and M_C phases (Fig. 2). Different orientations of the spontaneous polarisation vectors in the adjacent domains of the aforementioned phases are listed in Table 1. In the T phase the following domain patterns are considered (Fig. 1): the first domain pattern comprises the 90° domains with the spontaneous polarisation vectors $\boldsymbol{P_T^{(3)}}\|[0\,0\,1]$, and the second domain pattern does not comprise the domains with $\boldsymbol{P_T^{(3)}}\|[0\,0\,1]$.

Distortion matrices of the polydomain (twinned) phases are written with respect to the rectangular co-ordinate axes (OX_j) shown in Figs. 1 and 2. These axes are assumed to be parallel to the perovskite unit-cell axes in the C phase. The distortion matrix of the T phase with the domains shown in Fig. 1(a) is written in the form

$$||N_{ij}^{(TA)}|| = (1-t_3)\begin{pmatrix} \varepsilon_c & 0 & 0 \\ 0 & \varepsilon_a & 0 \\ 0 & 0 & \varepsilon_a \end{pmatrix} + t_3 \begin{pmatrix} \cos\varphi_t & 0 & -\sin\varphi_t \\ 0 & 1 & 0 \\ \sin\varphi_t & 0 & \cos\varphi_t \end{pmatrix} \begin{pmatrix} \varepsilon_a & 0 & 0 \\ 0 & \varepsilon_a & 0 \\ 0 & 0 & \varepsilon_c \end{pmatrix}. \quad (1)$$

The T phase split into the domains shown in Fig. 1(b) is described by the distortion matrix

$$||N_{ij}^{(TB)}|| = (1-t_1)\begin{pmatrix} \varepsilon_a & 0 & 0 \\ 0 & \varepsilon_c & 0 \\ 0 & 0 & \varepsilon_a \end{pmatrix} + t_1 \begin{pmatrix} \cos\varphi_t & -\sin\varphi_t & 0 \\ \sin\varphi_t & \cos\varphi_t & 0 \\ 0 & 0 & 1 \end{pmatrix} \begin{pmatrix} \varepsilon_c & 0 & 0 \\ 0 & \varepsilon_a & 0 \\ 0 & 0 & \varepsilon_a \end{pmatrix}. \quad (2)$$

In Eqs. (1) and (2) ε_a and ε_c are unit-cell distortions and $\varphi_t = \arccos[2\varepsilon_a\varepsilon_c/(\varepsilon_a^2 + \varepsilon_c^2)]$ is an angle that describes a rotation of the crystallographic axes of the adjacent domains in the T phase. The distortion matrix of the polydomain M_B phase (Fig. 2(a)) is written as

$$||N_{ij}^{(MB)}|| = (1-y_B)\begin{pmatrix}\lambda_c & 0 & 0\\ 0 & \lambda_a & \lambda(2u_B-1)\\ 0 & \lambda(2u_B-1) & \lambda_a\end{pmatrix} + y_B\begin{pmatrix}\cos\varphi_B & -\sin\varphi_B & 0\\ \sin\varphi_B & \cos\varphi_B & 0\\ 0 & 0 & 1\end{pmatrix} \times \begin{pmatrix}\lambda_a & 0 & \lambda(2u_B-1)\\ 0 & \lambda_c & 0\\ \lambda(2u_B-1) & 0 & \lambda_a\end{pmatrix} \quad (3)$$

where λ_a, λ_c and λ are unit-cell distortions and $\varphi_B = \arccos[2\lambda_a\lambda_c/(\lambda_a^2+\lambda_c^2)]$ is the rotation angle like φ_t introduced in Eqs. (1) and (2). The distortion matrix of the polydomain M_C phase (Fig. 2(b)) has the form

$$||N_{ij}^{(MC)}|| = (1-y_C)\begin{pmatrix}\eta_b & 0 & 0\\ 0 & \eta_a & \eta(2u_C-1)\\ 0 & \eta(2u_C-1) & \eta_c\end{pmatrix} + y_C\begin{pmatrix}\cos\varphi_C & -\sin\varphi_C & 0\\ \sin\varphi_C & \cos\varphi_C & 0\\ 0 & 0 & 1\end{pmatrix} \times \begin{pmatrix}\eta_a & 0 & \eta(2u_C-1)\\ 0 & \eta_b & 0\\ \eta(2u_C-1) & 0 & \eta_c\end{pmatrix} \quad (4)$$

where η_a, η_b, η_c, and η are unit-cell distortions and $\varphi_C = \arccos[2\eta_a\eta_b/(\eta_a^2+\eta_b^2)]$ is the rotation angle. The C paraelectric phase is assumed to be unstrained, and its distortion matrix equals the unit 3×3 matrix.

Based on the algorithm [3,4,6], we approximate an interface between the coexisting phases by a second-degree surface

$$\sum_{a,b=1}^{3} D_{ab}x_a x_b = 0 \quad (5)$$

where matrix elements

$$D_{ab} = \sum_{f=1}^{3}(N_{af}^{(II)}N_{bf}^{(II)} - N_{af}^{(I)}N_{bf}^{(I)}) \quad (6)$$

are written in terms of the distortion matrices $\left\|N_{af}^{(I)}\right\|$ and $\left\|N_{af}^{(II)}\right\|$ of the coexisting phases I and II.[1] In our study the matrices $\left\|N_{af}^{(I)}\right\|$ and $\left\|N_{af}^{(II)}\right\|$ are chosen in pairs among those represented by Eqs. (1)–(4). The interfaces separating the phases are classified taking into account signs of invariants [3,4] of Eq. (5)

$$I = D_{11}+D_{22}+D_{33},\ D = \det||D_{ab}|| \quad \text{and}$$

$$J = \begin{vmatrix}D_{11} & D_{12}\\ D_{21} & D_{22}\end{vmatrix} + \begin{vmatrix}D_{22} & D_{23}\\ D_{32} & D_{33}\end{vmatrix} + \begin{vmatrix}D_{33} & D_{31}\\ D_{13} & D_{11}\end{vmatrix}. \quad (7)$$

Eqs. (7) have been written in terms of the matrix elements from Eq. (6). Conditions $DI<0$ and $J<0$ (region I), $DI<0$ and $J>0$ (region II), and $DI>0$ and $J<0$ (region III) are satisfied for conical interfaces. Inequalities $DI>0$ and $J>0$ (region IV) correspond to an apex of an imaginary cone. In the general case invariants (7) are functions of some parameters (for example, t_j, u_B and y_B) which determine volume fractions of different domain types (Figs. 1 and 2) in the coexisting phases.

The conditions

$$DI = 0 \quad \text{and} \quad J < 0, \quad (8)$$

which are fulfilled on a line between regions I and III, correspond to interfaces being zero-net-strain planes (ZNSPs). An elastic matching of the coexisting phases along the ZNSP provides complete mechanical stress relief in the heterophase structures. This means that vanishing excessive elastic energy are a result of spontaneous strains and jump-like changes in the unit-cell parameters at the first-order phase transition. In the sections below we consider some important examples of heterophase states and interfaces between the phases coexisting in the PMN–*x*PT system.

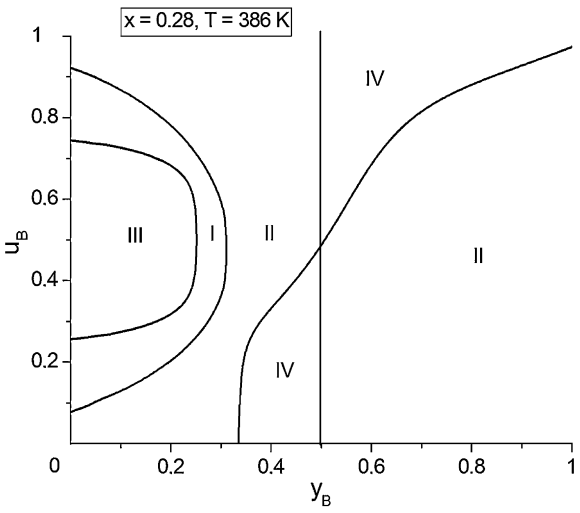

Fig. 3. Domain state–interface diagram for the C–M_B phase transition in PMN–0.28PT. u_B and y_B are parameters that characterise volume fractions of domains (Fig. 2(a)) in the M_B phase. Calculations have been made using the experimental unit-cell parameters [9].

3. Monoclinic phases in heterophase PMN–*x*PT (*x* = 0.28, 0.32 and 0.34)

3.1. C–M_B phase coexistence

As follows from experimental data [9], the first-order C–M_B phase transition is observed in PMN–0.28PT at temperature $T_{CB} = 388 \pm 5$ K. The corresponding domain state–interface diagram shown in Fig. 3 suggests that a line separating regions I and III obeys conditions (8). It means that the interfaces being ZNSPs can appear in the presence of either two ($y_B = 0$) or four ($y_B \neq 0$) domain types represented in Fig. 2(a). It is noteworthy that the optimum volume fraction parameters of the domains in the M_B phase obeying conditions for complete stress relief are varied in relatively wide ranges: $0 < y_B^{opt} < 1/4$ and $1/4 < u_B^{opt} < 3/4$ (Fig. 3). Such variations would promote an effective stress accommodation in the heterophase system. Vast regions I, II and III in the same diagram shown in Fig. 3 are related to conical C–M_B interfaces which provide partial stress relief only.

3.2. T–M_B phase coexistence

According to experimental results [9], zero-field cooled samples of PMN–0.32PT undergo the first-order C–T phase transition at temperature $T_{CT} = 423 \pm 5$ K and show the T–M_B phase coexistence in the temperature range of 193 K $\leq T \leq$ 408 K. Based on X-ray diffrac-

[1] It should be noted that notations of the coexisting phases I and II are not concerned with domain types I–IV shown in Figs. 1 and 2 and regions I–IV in Figs. 3–6.

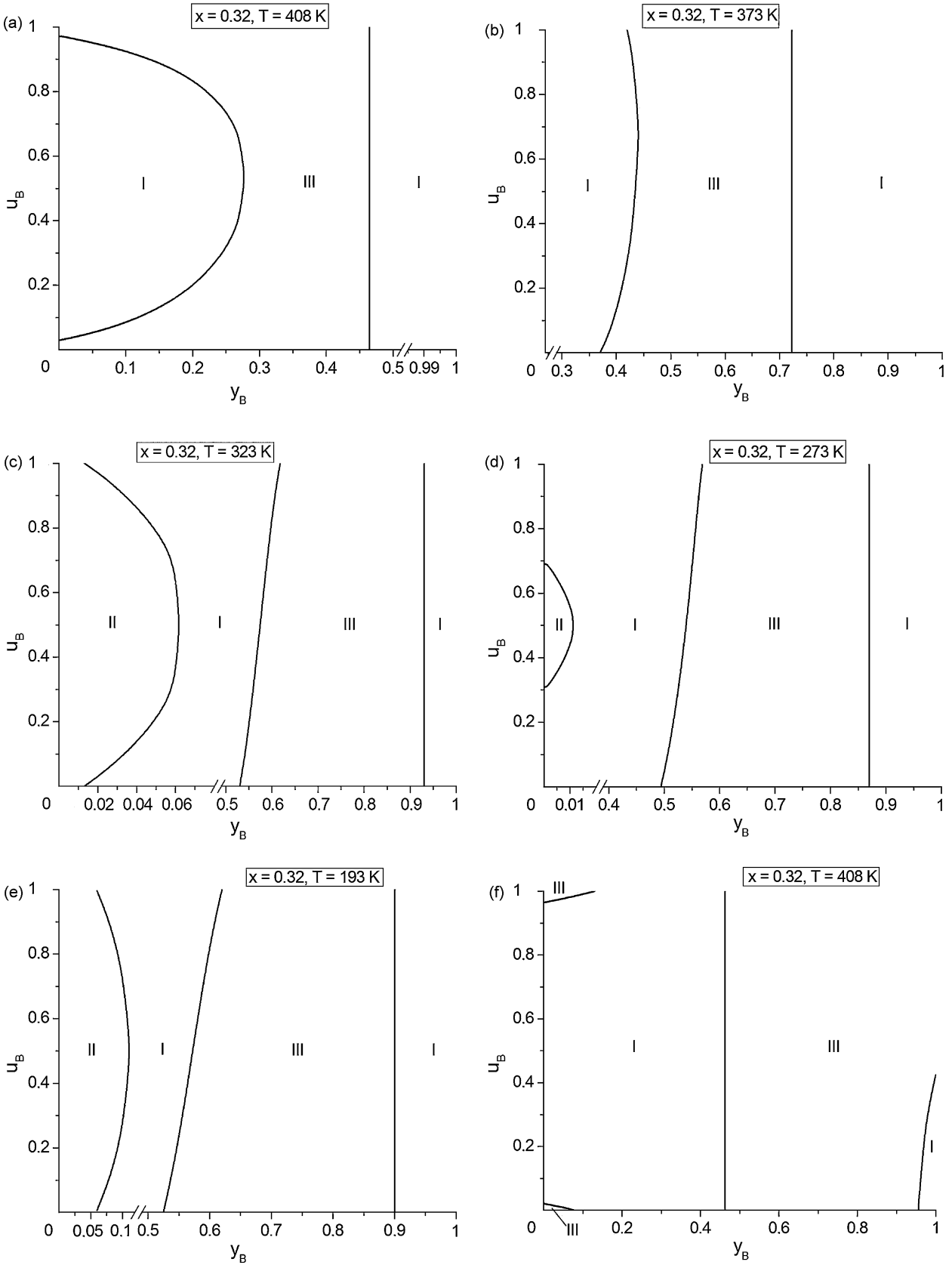

Fig. 4. Domain state–interface diagrams for the T–M_B phase transition in PMN–0.32PT with different domain patterns in the T phase. Graphs (a)–(e) correspond to the transition from the polydomain T phase (Fig. 1(a)) at $t_3 = 0.313$, graph (f) corresponds to the transition from the polydomain T phase (Fig. 1 (a)) at $t_3 = 0.687$, and graph (g) corresponds to the transition from the polydomain T phase (Fig. 1(b)) at $t_1 = 0.313$. u_B and y_B are parameters that characterise volume fractions of domains (Fig. 2(a)) in the M_B phase. Calculations have been made using the experimental unit-cell parameters [9].

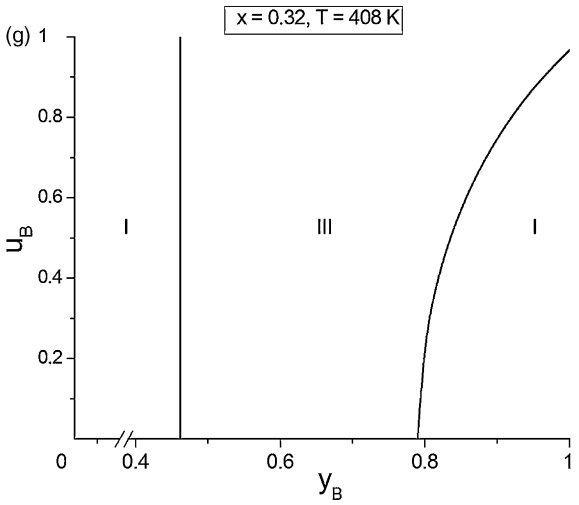

Fig. 4. (*Continued*).

tion data, Li et al. emphasised [9] a non-equilibrium character of this T–M_B phase coexistence.

Our analysis of conditions (8) for the C–T phase transition shows that the interfaces separating the C paraelectric phase and the T ferroelectric phase split into domains (see Fig. 1) can be ZNSPs at the optimum volume fraction of these domains $t_j^{opt} = \xi_c^s/(\xi_c^s - \xi_a^s)$, where $\xi_a^s = \varepsilon_a - 1$ and $\xi_c^s = \varepsilon_c - 1$ are spontaneous strains of the perovskite unit cell, ε_a and ε_c are unit-cell distortion from Eqs. (1) and (2) and $j = 1$, 2 or 3. Changes in the unit-cell parameters of PMN–0.32PT at the C–T phase transition [9] lead to $t_j^{opt} =$ 0.313 or 0.687.

It is assumed that a further cooling of the sample in the stability region of the T phase does not give rise to changes in the volume fractions of the domains which have been formed at the C–T phase transition. This means that distortions from Eqs. (1) and (2) are written at $t_j = t_j^{opt}$. The M_B phase separation into domains, as shown in Fig. 2(a), is described by the distortion matrix from Eq. (3). Examples of the domain state–interface diagrams calculated for the T–M_B phase coexistence at $t_j = t_j^{opt}$ are shown in Fig. 4. The diagrams shown in Fig. 4(a), (f) and (g) correspond to the highest temperature ($T = 408$ K) at which the unit-cell parameters of the coexisting T and M_B phases have been measured [9]. It is seen from these diagrams (Fig. 4(a), (f) and (g)) that, irrespective of the domain pattern in the high-temperature T phase, the almost single-domain M_B phase would appear to satisfy conditions (8) and, therefore, to provide complete stress relief. This M_B phase is characterised by the parameters $y_B = 0$ and $u_B \to 0$ or $y_B = 0$ and $u_B \to 1$ (see the curves separating regions I and III in Fig. 4(a) and (f)), $y_B \to 0$ and $u_B = 1$ (see the curve separating regions I and III in Fig. 4(f)), and $y_B = 0$ and $u_B \to 1$ (see the curve separating regions I and III in Fig. 4(g)). Moreover, the diagram shown in Fig. 4(a) suggests an interesting possibility of forming the polydomain M_B phase with the parameters $y_B \to t_3 = 0.313$ and $u_B = 1/2$. In this case the ZNSP would appear in the heterophase structure with almost constant relative thickness of the domains or twins along the OX_1 axis (compare the domain patterns shown in Figs. 1(a) and 2(a)).

It is also important to compare the diagrams (Fig. 4(a)–(e)) which are related to the fixed orientation of the domains in the T and M_B phases coexisting in the wide temperature range on cooling. It turns out that each single-domain state of the M_B phase expected at $T = 408$ K can give rise to excessive mechanical stress at the interfaces on cooling. For example, the corresponding T–M_B interfaces are to be conical (region I or II) at $T = 373$ K (Fig. 4(b)), 323 K (Fig. 4(c)), 273 K (Fig. 4(d)), or 193 K (Fig. 4(e)). This stress-relief path needs additional changes in volume fractions of the domains in the T phase (Fig. 1(a)) that has been thermodynamically stable at higher temperatures.

The aforementioned polydomain M_B phase with the parameters $y_B \to t_3 = 0.313$ and $u_B = 1/2$ (Fig. 4(a)) also promote the formation of stressed conical interfaces on cooling. The curve separating regions I and III in the left part of the diagram (Fig. 4(a)) shifts to larger y_B values (Fig. 4(b) and (c)) and then shows small displacements (Fig. 4(d) and (e)). The corresponding scenario means that an additional rearrangement of the domain structure shown in Fig. 2(a) can be appreciable down to $T \approx 320$ K at the constant volume fractions t_j^{opt} and $1 - t_j^{opt}$ of the domains in the T phase.

It is probable that the samples of PMN–0.32PT [9] cooled below $T = 408$ K remain heterophase in the wide temperature range without effective stress relief and accommodation of the domain structure in both the polydomain phases, T and M_B. Additional reasons of the T–M_B phase coexistence in the wide temperature range [9] may be due to compositional fluctuations close to the morphotropic phase boundary and with a presence of different orientation states of domain (twins) in different parts of a sample. It seems probable that complicated domain structures formed independently in different parts of the sample on cooling need "more individual" conditions for stress relief when mechanical stress fields of neighbouring regions are to be taken into account.

An important feature of the diagrams calculated for PMN–0.34PT (Fig. 5) is the presence of almost vertical lines which separate regions I and III and correspond to ZNSPs. In both cases at $u_B = 0$, the lower volume fraction parameter y_B (Fig. 5) approximately equals the optimal volume fraction t_3^{opt} (Fig. 1) as determined for the previous C–T phase transition. This promotes a coexistence of the T and M_B phases, each separated into two domain types, with almost equal relative widths of the domains in these phases. Such conditions for complete stress relief have no analogues among those considered [3,6] in PMN–*x*PT near the morphotropic phase boundary.

3.3. T–M_C phase coexistence

A temperature dependence of the perovskite unit-cell parameters of PMN–0.32PT has also been determined in the powder neutron diffraction study [11]. This temperature dependence predetermines another scenario of stress relief in comparison with that described in Section 3.2. Based on the unit-cell parameters from work [11], the C–T interfaces are determined to be ZNSPs at the

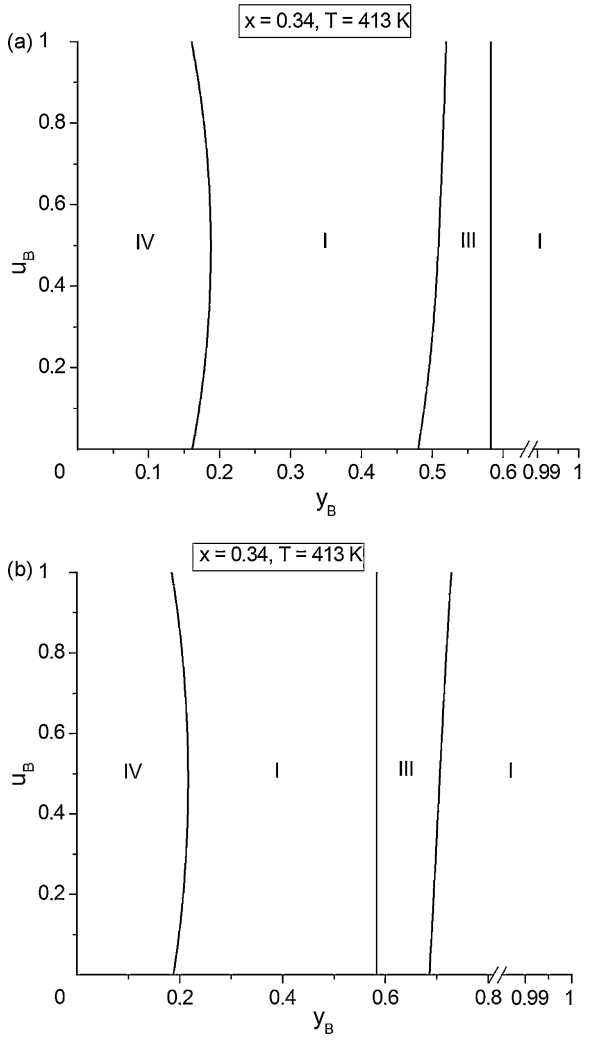

Fig. 5. Domain state–interface diagrams for the T–M_B phase transition in PMN–0.34PT. Graph (a) corresponds to the transition from the polydomain T phase (Fig. 1(b)) at $t_3 = 0.423$, graph (b) corresponds to the transition from the polydomain T phase (Fig. 1(a)) at $t_3 = 0.577$. u_B and y_B are parameters that characterise volume fractions of domains (Fig. 2(a)) in the M_B phase. Calculations have been made using the experimental unit-cell parameters [9].

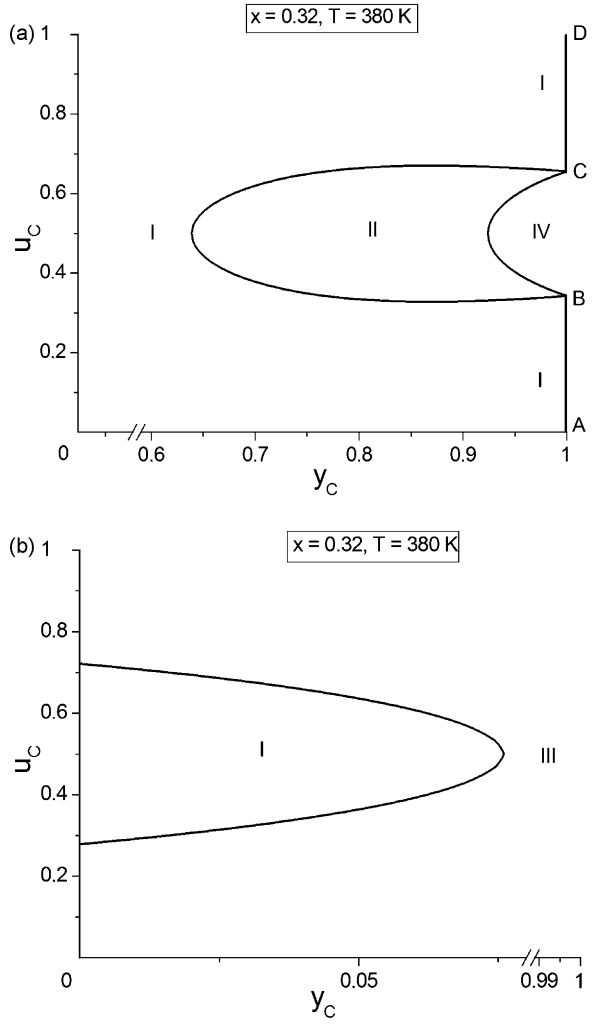

Fig. 6. Domain state–interface diagrams for the T–M_C phase transition in PMN–0.32PT. Graph (a) corresponds to the transition from the polydomain T phase (Fig. 1(b)) at $t_3 = 0.595$, graph (b) corresponds to the transition from the polydomain T phase (Fig. 1(b)) at $t_1 = 0.405$. u_C and y_C are parameters that characterise volume fractions of domains (Fig. 2(b)) in the M_C phase. Calculations have been made using the experimental unit-cell parameters [11].

volume fractions of the 90° domains (Fig. 1) $t_j^{opt} = 0.405$ or 0.595. The polydomain M_C phase (Fig. 2(b)) that appears on further cooling is characterised by the distortion matrix from Eq. (4). The domain state–interface diagrams (Fig. 6) calculated using the unit-cell parameters [11] at the T–M_C phase transition suggest that conditions (8) are fulfilled in the presence of the M_C phase being either single-domain or polydomain.

Of specific interest are lines AB and CD (Fig. 6(a)) and AD (Fig. 6(b)) which correspond to the ZNSPs. The single-domain M_C phase is related to points A and D in Fig. 6. The M_C phase split into two domain types is described by lines AB and CD (Fig. 6(a)) and AD (Fig. 6(b)) with the exception of points A ($y_C = 1$ and $u_C = 0$) and D ($y_C = u_C = 1$) in both the diagrams. Moreover, the curve separating regions I and III in Fig. 6(b) corresponds to the ZNSPs which take place in the presence of the M_C phase split into either two (at $y_C = 0$) or four (at $y_C > 0$) domain types. Undoubtedly, these variants of the T–M_C phase coexistence in PMN–0.32PT are related to similar stress-relief trends at different domain patterns of the T phase with the optimum volume fractions t_j^{opt} and $1 - t_j^{opt}$ of the domains.

4. Conclusions

The present study on heterophase states in PMN–*x*PT and the domain state–interface diagrams proposed for this system have provided insight into the intermediate monoclinic (M_B or M_C) phases and understanding of stress-relief conditions at phase coexistence near the morphotropic phase boundary. Two variants of the temperature dependence of the unit-cell parameters determined in experimental work by Li et al. [9] and Singh et al. [11] enabled us to predict different scenarios of stress relief in heterophase samples wherein different non-180° domain types (twins) play the active role. Domain structures corresponding to complete stress relief for different compositions suggest that there is a correlation between the unit-cell parameters of the adjacent phases (i.e. C, T, M_B, and M_C) in certain temperature ranges. This correlation causes, for example, possibilities of forming the single-domain monoclinic phase (either M_B or M_C) at the first-order phase transition from the T phase that has been split into domains in accordance with conditions for ZNSPs at the high-temperature C–T phase transition. It is believed that such and like causal relationships can be taken into account by studying different sequences of phase transitions in solid solutions near the morphotropic phase boundary. It is also believed that

behaviour of the unit-cell parameters near the morphotropic phase boundary provides not only favourable stress-relief conditions in the vast x and T ranges, but also leads to important electromechanical properties in the heterophase PMN–xPT solid solutions.

Acknowledgments

The author is grateful to Prof. Dr. A.V. Turik, Prof. Dr. V.G. Gavrilyachenko and Prof. Dr. A.E. Panich (Rostov-on-Don, Russia), Prof. Dr. Z.-G. Ye (Burnaby, BC, Canada), Prof. Dr. D. Viehland and Dr. H. Cao (Blacksburg, VA, USA) for their constant interest in the research problems. The author thanks Dr. C.R. Bowen (Bath, UK) for careful reading of the manuscript. This work was supported by the administration of the Southern Federal University and by the Ministry of Education and Science of the RF (*Development of the Scientific Potential of the Higher School*, the purpose-oriented programme, project code 2786), and this support is gratefully acknowledged.

References

[1] B. Noheda, Curr. Opin. Solid State Mater. Sci. 6 (2002) 27.
[2] Z.-G. Ye, V. Yu Topolov, Ferroelectrics 253 (2001) 79.
[3] V.Yu. Topolov, Phys. Solid State 48 (2006) 1334.
[4] V.Yu. Topolov, H. Cao, D. Viehland, J. Phys.: Condens. Matter 19 (2007) 246224.
[5] Z.-G. Ye, J. Dong, J. Appl. Phys. 87 (2000) 2312.
[6] V.Yu. Topolov, Z.-G. Ye, Phys. Rev. B 70 (2004) 094113.
[7] C.-S. Tu, L.-L. Tsai, J.-S. Chen, V.H. Schmidt, Phys. Rev. B 65 (2002) 104113.
[8] A. Singh, D. Pandey, Phys. Rev. B 67 (2003) 064102.
[9] J.-B. Li, G.H. Rao, G.Y. Liu, J.R. Chen, L. Lu, X. Jing, S. Li, J.K. Liang, J. Alloys Compd. 425 (2006) 373.
[10] V.Yu. Topolov, H. Cao, D. Viehland, J. Appl. Phys. 102 (2007) 024103.
[11] A. Singh, D. Pandey, O. Zakharko, Phys. Rev. B 74 (2006) 024101.
[12] B. Noheda, D.E. Cox, G. Shirane, J. Guo, Z.-G. Ye, Phys. Rev. B 66 (2002) 054104.
[13] V.A. Shuvaeva, A.M. Glazer, D. Zekria, J. Phys.: Condens. Matter 17 (2005) 5709.
[14] Y.M. Jin, Y.U. Wang, A.G. Khachaturyan, J.F. Li, D. Viehland, J. Appl. Phys. 94 (2003) 3629.
[15] D. Viehland, J. Appl. Phys. 88 (2000) 4794.
[16] J. Fousek, V. Janovec, J. Appl. Phys. 40 (1969) 135.